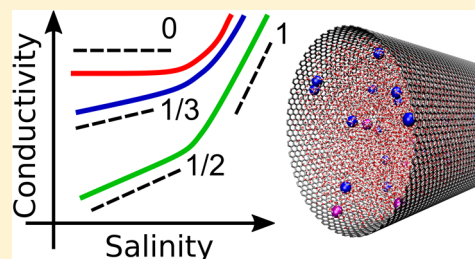


Crossover of the Power-Law Exponent for Carbon Nanotube Conductivity as a Function of Salinity

Yuki Uematsu,^{†,‡} Roland R. Netz,[‡] Lydéric Bocquet,[§] and Douwe Jan Bonthuis^{*,‡}[†]Department of Chemistry, Kyushu University, Fukuoka 819-0395, Japan[‡]Fachbereich Physik, Freie Universität Berlin, 14195 Berlin, Germany[§]Laboratoire de Physique Statistique, École Normale Supérieure-PSL Research University, UMR 8550, 24 rue Lhomond, 75005 Paris, France

ABSTRACT: On the basis of the Poisson–Boltzmann equation in cylindrical coordinates, we calculate the conductivity of a single charged nanotube filled with electrolyte. The conductivity as a function of the salt concentration follows a power-law, the exponent of which has been controversially discussed in the literature. We use the co-ion-exclusion approximation and obtain the crossover between different asymptotic power-law behaviors analytically. Numerically solving the full Poisson–Boltzmann equation, we also calculate the complete diagram of exponents as a function of the salt concentration and the pH for tubes with different radii and pK_a values. We apply our theory to recent experimental results on carbon nanotubes using the pK_a as a fit parameter. In good agreement with the experimental data, the theory shows power-law behavior with the exponents 1/3 at high pH and 1/2 at low pH, with a crossover depending on salt concentration, tube radius and pK_a .



INTRODUCTION

The ionic transport of electrolyte solutions confined to nanochannels and nanotubes shows different behavior from that of the bulk electrolyte. Examples include surface conduction,¹ fast proton transport,² rectification,³ permselectivity,⁴ and block–unblock transport.^{5–7} In this work, we focus on the salinity dependence of the ionic conductivity. Stein et al. observed that at high salinity the conductivity (denoted by K) of 50 μm -wide silica nanochannels is proportional to the bulk salt concentration c_0 ($K \sim c_0$), whereas at low salinity the conductivity becomes constant ($K \sim \text{const.}$) and is governed by the surface charge density of the channel walls.¹ Since at low salinity the number of charge carriers in the channel equals the surface charge, the saturation of K can be understood by assuming the surface charge density to be independent of salinity. However, the surface charge is usually governed by the dissociation of protons from acidic groups, as well as by adsorption of ions from the solution, and is therefore expected to depend on c_0 .⁸ In the presence of such charge regulation, scaling laws $K \sim c_0^\gamma$ are expected with exponents γ different from 0 or 1. Such scaling laws of conductivity with $\gamma \neq 0$ and $\gamma \neq 1$ have been reported in experiments on track-etched membranes,^{9,10} biological membrane pores,^{11–13} silicon-dioxide nanopores,¹⁴ and single-walled carbon nanotubes.^{15–18} Recently, experiments by Secchi et al. demonstrated that the conductivity of a single multiwalled carbon nanotube obeys a power law as a function of salinity with exponent $\gamma = 1/3$.¹⁹ Later, Biesheuvel et al. theoretically derived a different power law with exponent $\gamma = 1/2$ at extremely low salinity.²⁰ Theoretical descriptions of the nanotube conductivity are based on the Poisson–Boltzmann (PB) equation in cylindrical coordinates, the analytical solution

of which is not simple.²¹ Therefore, all previous discussions of the conductivity at low salinity have considered approximations of the PB equation in cylindrical coordinates, for example the Donnan approximation,^{19,22} the co-ion-exclusion approximation,^{23,24} the planar approximation,^{25,26} or the linear approximation.²⁷ Yet the complete problem features many competing length scales, such as the Debye length, the Bjerrum length, the Gouy–Chapman length, the Stokes radius of the ions, and the radius of the nanotube, and a careful consideration of the validity of each approximation is paramount. Recently, Manghi et al. have analytically revealed that small values of the surface charge density give rise to the exponent 1/2 and large values give rise to the exponent 1/3 at low salinity, as well as another exponent 2/3 induced by hydrodynamic surface slip.²⁸ In their model, the scaling with $\gamma = 1/3$ does not appear within the experimentally accessible range of surface charge densities, however.

In this work, we numerically solve the PB equation in cylindrical coordinates, modeling both charge regulation and ion adsorption by the Langmuir adsorption isotherm.²⁹ In addition, we globally analyze the local exponent $\gamma = d \ln K / d \ln c_0$ as a function of pH and salt concentration. Using the co-ion-exclusion approximation, we analytically derive the crossover boundaries between the regions characterized by the exponents $\gamma = 0, 1/3, 1/2$, and 1 and show that they agree with the full numerical solution. Using the pK_a as a fit parameter, we argue that the experimental data¹⁹ show the predicted crossover from $\gamma = 1/3$ to $\gamma = 1/2$ with decreasing pH.

Received: February 26, 2018

Published: February 28, 2018

THEORY

Model. We consider a single nanotube with radius R filled with electrolyte connected to a reservoir. The electrostatic potential $\psi(r)$ is determined by the Poisson–Boltzmann equation in cylindrical coordinates as follows:

$$\frac{1}{r} \frac{d}{dr} \left[r \frac{d}{dr} \Psi(r) \right] = \kappa^2 \sinh \Psi(r) \quad (1)$$

where r is the radial coordinate, $\Psi(r) = e\psi/k_B T$ is the dimensionless electrostatic potential, κ is the inverse Debye length defined via $\kappa^2 = 2e^2 c_0 / \epsilon \epsilon_0 k_B T$, e is the elementary charge, $k_B T$ is the thermal energy, c_0 is the reservoir salt concentration at $\psi = 0$, ϵ is the dielectric constant of the solution, and ϵ_0 is the dielectric permittivity of vacuum. When we solve eq 1 with a constant surface potential $\Psi_R = e\psi(R)/k_B T$ and $d\Psi/dr|_{r=0} = 0$ as boundary conditions, we obtain the potential profile $\Psi(r)$ and the surface charge density $\sigma = \epsilon \epsilon_0 d\psi/dr|_{r=R}$.

To determine the surface potential, we use the Langmuir adsorption isotherm including the effect of the surface potential,

$$\sigma = -e\Gamma_{\text{site}} \frac{e^{\Psi_R} 10^{\text{pH} - \text{p}K_a}}{1 + e^{\Psi_R} 10^{\text{pH} - \text{p}K_a}} \quad (2)$$

where pH is the pH of the reservoir, $\text{p}K_a$ is the deprotonation reactivity of the surface, and Γ_{site} is the surface density of dissociable sites. The charging mechanism for hydrophobic surfaces is still under debate,^{30–35} but using different equilibrium constants, the same functional form can be used to model the surface adsorption of ions such as OH^- or charged impurities from the solution.³²

When we assume that all the ions in the solution have the same ionic mobility, then the conductivity is given by the following:

$$K = \frac{e^2}{8\eta(\pi l_B R)^2} \int_0^R \left[\frac{d\Psi}{dr} \right]^2 r dr + \frac{4e\nu_0 c_0}{R^2} \int_0^R \cosh \Psi(r) r dr \quad (3)$$

where η is the viscosity of the solution, $l_B = e^2/4\pi\epsilon\epsilon_0 k_B T$ is the Bjerrum length, and ν_0 is the ionic electrophoretic mobility in the solution. We call the first term of eq 3 the convective part K_{cv} and the second term of eq 3 the conductive part K_{cd} . Note that the nanotube conductivity is additionally influenced by interfacial effects such as surface slip and the inhomogeneity of the dielectric constant, as well as the effects of confinement on the bulk dielectric constant, viscosity, and ionic mobility. To preserve the analytical tractability of the asymptotic expressions, we neglect these effects in this work. If the length of the nanotube is short compared to the radius, then the conductance of the inlet and outlet of the nanotube dominates the total conductance.^{36,37} In this work, however, we assume the length to be long enough to neglect the entrance effects. The validity of the continuum model is expected to be limited to radii that are large compared to the atomic length scale. The fact that nanotubes of $R = 0.8$ nm also show power-law conductivity¹⁷ suggests that this lower bound has not been reached.

To evaluate the conductivity, we need to solve eq 1. However, the analytical expression of the exact solution is not simple,²¹ and only some asymptotic solutions are available. Therefore, we use the co-ion-exclusion approximation^{23,24} to derive the asymptotic scaling laws analytically. To verify the validity of this approximation, we also solve eq 1 numerically.

Co-ion-exclusion Approximation. The co-ion-exclusion approximation is valid when $c^-(r)/c^+(r) = e^{2\Psi(r)} \ll 1$ for all r , with $c^{\pm}(r)$ being the concentrations of cations and anions. Neglecting

the contribution of the co-ions in eq 1, $\Psi(r)$ satisfies the following:

$$\frac{1}{r} \frac{d}{dr} \left[r \frac{d}{dr} \Psi(r) \right] = -\frac{\kappa^2}{2} e^{-\Psi(r)} \quad (4)$$

The exact solution of eq 4 is given by the following:^{23,24}

$$\Psi(r) = \ln \frac{\kappa^2 R^2 [1 + \Sigma - \Sigma(r/R)^2]^2}{16\Sigma(1 + \Sigma)} \quad (5)$$

where the rescaled radius is given by the following:

$$\Sigma = \frac{R}{2l_{\text{GC}}} = \frac{R\epsilon l\sigma}{4e\epsilon_0 k_B T} \quad (6)$$

with the Gouy–Chapman length being defined by $l_{\text{GC}} = 2e\epsilon_0 k_B T / e l\sigma$. In the co-ion-exclusion regime, l_{GC} provides a measure of the width of the ion distribution at the charged interface, and therefore Σ characterizes the extent of counterion binding to the nanotube surface. Equation 5 gives the surface potential as follows:

$$\Psi_R = \ln \frac{\kappa^2 R^2}{16\Sigma(1 + \Sigma)} \quad (7)$$

Using the potential of eq 5, we calculate the conductive part of the conductance by eq 3,

$$K_{\text{cd}}^+ = \frac{4e\nu_0 c_0}{R^2} \int_0^R \frac{e^{-\Psi(r)}}{2} r dr = \frac{2\nu_0 |\sigma|}{R} \quad (8)$$

$$\begin{aligned} K_{\text{cd}}^- &= \frac{4e\nu_0 c_0}{R^2} \int_0^R \frac{e^{\Psi(r)}}{2} r dr \\ &= e\nu_0 c_0 \frac{\kappa^2 R^2}{16\Sigma(1 + \Sigma)} \left(1 + \Sigma + \frac{\Sigma^2}{3} \right), \end{aligned} \quad (9)$$

where K_{cd}^{\pm} is the cation (anion) contribution to K_{cd} , and $K_{\text{cd}} = K_{\text{cd}}^+ + K_{\text{cd}}^-$. For the convective part of the conductivity, eq 3 yields the following:

$$\begin{aligned} K_{\text{cv}} &= \frac{\sigma^2}{2\eta} \left[\frac{2}{\Sigma} \left(1 - \frac{\ln(1 + \Sigma)}{\Sigma} \right) \right] \\ &= \frac{2\nu_0 |\sigma|}{R} \frac{3l_S}{l_B} \left(1 - \frac{\ln(1 + \Sigma)}{\Sigma} \right), \end{aligned} \quad (10)$$

where in the second line the equation has been rewritten in terms of the ionic Stokes radius $l_S = e/6\pi\eta\nu_0$. In the limit of $\Sigma \ll 1$ (corresponding to $R \ll 2l_{\text{GC}}$), the total conductivity, given by the sum of eqs 8, 9, and 10, becomes the following:

$$K \approx \frac{2\nu_0 |\sigma|}{R} \left(1 + \frac{\kappa^4 R^4}{128\Sigma^2} + \frac{3l_S \Sigma}{2l_B} \right) \quad (11)$$

whereas in the limit of $\Sigma \gg 1$ (corresponding to $R \gg 2l_{\text{GC}}$), we obtain the following:

$$K \approx \frac{2\nu_0 |\sigma|}{R} \left(1 + \frac{\kappa^4 R^4}{768\Sigma} + \frac{3l_S}{l_B} \right) \quad (12)$$

To check the self-consistency of the co-ion-exclusion approximation, we now verify the condition $e^{2\Psi(r)} \ll 1$. Since $\Psi(r)$ is a monotonic function, we need to check only whether $e^{2\Psi(0)} \ll 1$, which by eq 5 becomes the following:

$$e^{2\Psi(0)} = \left[\frac{\kappa^2 R^2 (1 + \Sigma)}{16\Sigma} \right]^2 = \left[\frac{\kappa R}{16} \right]^2 (2\kappa l_{GC} + \kappa R)^2 \ll 1 \quad (13)$$

Equation 13 is fulfilled at low salt concentration ($\kappa R \ll 1$ and $\kappa l_{GC} \ll 1$), but also depends on the surface charge density and the nanotube radius in a nontrivial way. If eq 13 holds, then the relative co-ion conductance also satisfies the following for both cases $\Sigma \ll 1$ and $\Sigma \gg 1$:

$$\frac{K_{cd}^-}{K_{cd}^+} = \left[\frac{\kappa R}{16} \right]^2 \left((2\kappa l_{GC})^2 + \frac{(\kappa R)^2}{3(1 + \Sigma)} \right) \ll 1 \quad (14)$$

which means that we may indeed calculate the conductivity using the co-ion-exclusion approximation.

Power-Law Behavior of the Conductivity in the Low Salt Regime. First, we study the asymptotic behavior of the adsorption isotherm, eq 2. The surface potential is always negative, $\Psi_R < 0$, and if the solution is sufficiently acidic such that,

$$\text{pH} \ll \text{p}K_a - \frac{\Psi_R}{\ln 10} \quad (15)$$

then the surface charge density can be expressed as follows:

$$\sigma \approx -e\Gamma_0 e^{\Psi_R} \quad (16)$$

where $\Gamma_0 = \Gamma_{\text{site}} 10^{\text{pH} - \text{p}K_a}$. Conversely, if the solution is sufficiently basic such that,

$$\text{pH} \gg \text{p}K_a - \frac{\Psi_R}{\ln 10} \quad (17)$$

then the surface charge density becomes constant and equal to the following:

$$\sigma \approx -e\Gamma_{\text{site}} \quad (18)$$

Next, we calculate the conductance for different combinations of surface charge and nanotube radius (quantified by Σ) at low pH, in which case eq 16 is valid. When $\Sigma \ll 1$ and the co-ion-exclusion approximation is valid (at low salinity) we obtain the following from eq 11

$$K \approx \frac{2\nu_0 |\sigma|}{R} \quad (19)$$

Note that in eq 19, the contribution from convection has vanished. Combining eqs 7 and 16 with $\Sigma \ll 1$ yields the following:

$$|\sigma| \approx \left(\frac{e^2 R \Gamma_0 c_0}{2} \right)^{1/2} \quad (20)$$

Substituting eq 20 into eq 19, we obtain the following:

$$K \approx \frac{2\nu_0}{R} \left(\frac{e^2 R \Gamma_0 c_0}{2} \right)^{1/2} \quad (21)$$

which shows a power-law dependence of K on c_0 with the exponent $\gamma = 1/2$.²⁰

When, conversely, $\Sigma \gg 1$ and the co-ion-exclusion approximation is valid (at low salinity), eq 12 becomes the following:

$$K \approx \frac{2\nu_0 |\sigma|}{R} \left(1 + \frac{3I_S}{I_B} \right) \quad (22)$$

which does include a convective contribution, contrary to eq 19. Combining eqs 7 and 16 with $\Sigma \gg 1$ yields the following:

$$\sigma \approx -(2\varepsilon\varepsilon_0 k_B T e \Gamma_0 c_0)^{1/3} \quad (23)$$

Substituting eq 23 into eq 22, we obtain the following:

$$K \approx \frac{2\nu_0}{R} \left(1 + \frac{3I_S}{I_B} \right) (2\varepsilon\varepsilon_0 k_B T e \Gamma_0 c_0)^{1/3} \quad (24)$$

which exhibits a power-law dependence of K on c_0 with the exponent $\gamma = 1/3$.¹⁹ This shows that the crossover between power-law exponents 1/2 and 1/3 is governed by the extent of counterion binding quantified by Σ .

Finally, we study the case of high pH, when the surface charge density becomes constant. In this limit, it follows from eq 18 that,

$$\Sigma \approx \pi l_B R \Gamma_{\text{site}} \gg 1 \quad (25)$$

Substituting eq 25 into eq 22, we obtain the following:

$$K \approx \frac{2\nu_0}{R} \left(1 + \frac{3I_S}{I_B} \right) e \Gamma_{\text{site}} \quad (26)$$

which is constant as a function of c_0 , and can be interpreted as a power law with the exponent $\gamma = 0$.

NUMERICAL RESULTS

In this section, we numerically solve eq 1 without any approximation and evaluate the conductivity K and the local exponent γ defined by the following:

$$\gamma(c_0, \text{pH}) = \frac{d \ln K}{d \ln c_0} \quad (27)$$

Then we check our theory described in the previous section by analytically calculating the boundaries between the four regimes of different asymptotic behavior ($\gamma = 0, 1/3, 1/2, \text{ and } 1$).

Figure 1 shows a color map of γ in the c_0 -pH plane for a nanotube with radius $R = 35$ nm calculated by numerically solving eq 1. To solve eq 1, we use $\varepsilon = 78$, $T = 298$ K, $\eta = 0.89$

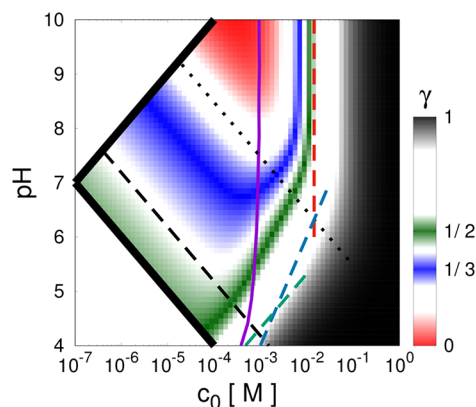


Figure 1. Color map of γ in the c_0 -pH plane for a nanotube of radius $R = 35$ nm. We use $\varepsilon = 78$, $T = 298$ K, $\eta = 0.89$ mPa·s, and $\nu_0 = 75$ cm²·S/(e·mol). We choose $\Gamma_{\text{site}} = 0.2/\text{nm}^2$ and $\text{p}K_a = 5.0$ in order to visualize the entire power-law sequence. The local exponent γ is calculated numerically, whereas the straight lines denote analytical results for the scaling boundaries. The black dotted line shows eq 28. The black broken line shows eq 29. The green broken line shows eq 30. The blue broken line shows eq 31. The red broken line shows eq 32. The purple line shows eq 33.

mPa·s, $R = 35$ nm, and $\nu_0 = 75$ cm²·S/(e ·mol) which satisfies $\nu_0 \approx (\nu_K + \nu_{Cl})/2$ where ν_K (ν_{Cl}) is the experimental value of the ionic mobility of potassium (chloride). For the charge regulation at the surface, we use $\Gamma_{\text{site}} = 0.2/\text{nm}^2$ and $\text{p}K_a = 5.0$, which have been chosen to ensure the appearance of the entire power-law sequence in a single figure. Note that we use different values for our comparison with experiments, where $\Gamma_{\text{site}} = 19/\text{nm}^2$ is estimated based on the carbon bond length and the $\text{p}K_a$ is used as a fit parameter. The region with $\gamma = 1$ is colored black, $\gamma = 1/2$ green, $\gamma = 1/3$ blue, and $\gamma = 0$ red. Determination of the scaling with c_0 in the region to the left of the black solid lines at low c_0 does not make sense because there the minimum salinity is determined by the pH of the solution. At high salinity, we observe the common behavior that $\gamma \rightarrow 1$, whereas at low salinity γ approaches either $1/2$, $1/3$, or 0 , depending on pH.

Boundaries between Different Asymptotic Regimes.

To determine the boundaries between the four regimes that display different asymptotic behavior, we further analyze our theory. The boundary between $\gamma = 0$ and $1/3$ is derived by combining eqs 18 and 23 with $\Sigma \gg 1$, giving the following:

$$c_0^{0 \rightarrow 1/3} \approx \frac{2\pi l_B \Gamma_{\text{site}}^2}{10^{\text{pH} - \text{p}K_a}} \quad (28)$$

We plot eq 28 by the black dotted line in Figure 1. It exhibits a slope of -1 in the c_0 -pH plane and accurately delineates the boundary between the blue and red regions obtained numerically.

The boundary between $\gamma = 1/3$ and $1/2$ is derived using $\Sigma \approx 1$ in eqs 6, 7, and 16 as follows:

$$c_0^{1/3 \rightarrow 1/2} \approx \frac{4}{\pi^2 R^3 l_B^2 \Gamma_{\text{site}}^2 10^{\text{pH} - \text{p}K_a}} \quad (29)$$

We plot eq 29 by the black broken line in Figure 1. It also shows a slope of -1 in the c_0 -pH plane and follows the boundary between the green and blue regions well.

The boundary between the bulk behavior, $\gamma = 1$, and either $\gamma = 1/2$, $1/3$, or 0 is determined by comparing the bulk conductivity $K_b = 2e\nu_0 c_0$ to each of the asymptotic conductivity formulas, eqs 21, 24, and 26. First, the boundary between $\gamma = 1$ and $1/2$ is given by the following:

$$c_0^{1 \rightarrow 1/2} \approx \frac{\Gamma_{\text{site}} 10^{\text{pH} - \text{p}K_a}}{2R} \quad (30)$$

Second, the boundary between $\gamma = 1$ and $1/3$ is given by the following:

$$c_0^{1 \rightarrow 1/3} \approx \frac{1}{\sqrt{2\pi}} \left(1 + \frac{3l_S}{l_B} \right)^{3/2} \left(\frac{\Gamma_{\text{site}} 10^{\text{pH} - \text{p}K_a}}{R^3 l_B} \right)^{1/2} \quad (31)$$

Third, the boundary between $\gamma = 1$ and 0 is given by the following:

$$c_0^{1 \rightarrow 0} \approx \left(1 + \frac{3l_S}{l_B} \right) \frac{\Gamma_{\text{site}}}{R} \quad (32)$$

We plot eqs 30, 31, and 32 by the green, blue, and red broken lines, respectively (each line separating the bulk region from the region with the corresponding color) in Figure 1. Note that eqs 30, 31, and 32 have different slopes in the c_0 -pH plane and together describe the boundary very well.

Finally, we examine the condition for the validity of the co-ion-exclusion approximation. The solid purple line in Figure 1 shows the following:

$$e^{2\Psi(0)} = 0.5 \quad (33)$$

where $\Psi(0)$ is the potential in the center of the nanotube calculated by eqs 1 and 2 without any approximation. In the regime left of the line, we have $e^{2\Psi(0)} < 0.5$, and thus the co-ion-exclusion approximation is valid. The region where $e^{2\Psi(0)} < 0.5$ overlaps with each of the regimes with power-law exponents $\gamma = 0$, $1/3$, and $1/2$, which means that a priori each of these scaling laws is expected to be visible for the corresponding combination of salt concentration and pH, depending on $\text{p}K_a$ and Γ_{site} of the nanotube. To the right of the purple line, the co-ion-exclusion approximation breaks down, but we see that the analytically calculated scaling boundaries with the $\gamma = 1$ region match the numerical results very well nonetheless.

COMPARISON WITH EXPERIMENTS

The circles in Figure 2 show the experimental conductivity data of single multiwalled carbon nanotubes of radii $R = 35$ nm (a)

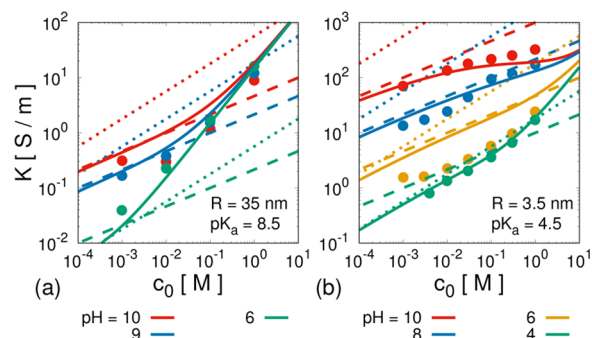


Figure 2. Conductivity of a single multiwalled carbon nanotube with radius $R = 35$ nm (a) and 3.5 nm (b). The points are the experimental data.¹⁹ The solid lines denote the numerical solution of eq 1 using (a) $\text{p}K_a = 8.5$ and (b) $\text{p}K_a = 4.5$. The broken lines are eq 24 exhibiting a slope of $\gamma = 1/3$, whereas the dotted lines denote eq 21 exhibiting a slope of $\gamma = 1/2$.

and 3.5 nm (b) and lengths 1.5 and 3 μm , respectively.¹⁹ We consider them long enough to neglect the inlet and outlet conductances. Since the charging mechanism of the carbon nanotube surface is still unclear, we assume that a dissociable site is located on every center of the carbon hexagons. On the basis of the bond length between carbons of 0.142 nm, the surface density of adsorbing sites is therefore $\Gamma_{\text{site}} = 19/\text{nm}^2$. We fit $\text{p}K_a$ by examining various values, $\text{p}K_a = 4.0, 4.5, \dots, 8.5, 9.0$, from which we obtain $\text{p}K_a = 8.5$ for $R = 35$ nm and $\text{p}K_a = 4.5$ for $R = 3.5$ nm, respectively, as best fits. Different $\text{p}K_a$ values for different radii implies a strong dependence of the charging mechanism on R . The solid lines denote the numerical solution of eq 1 by using the fitted $\text{p}K_a$ value. The broken and dotted lines denote the analytic asymptotic scaling predictions eqs 24 and 21, exhibiting the exponents $\gamma = 1/3$ and $1/2$, respectively.

For $R = 35$ nm, as shown in Figure 2a, the solid lines agree well with the experimental data. In the cases $\text{pH} = 9$ and 10 (red and blue), the solid lines approach the broken lines eq 24, which exhibit the exponent $\gamma = 1/3$ at low salinity. In contrast, at $\text{pH} = 6$ (green), the solid line approaches the dotted line ($\gamma = 1/2$) at low salinity, in agreement with our theoretical predictions. To show the crossover from $\gamma = 1/3$ to $1/2$ for a given pH value, however,

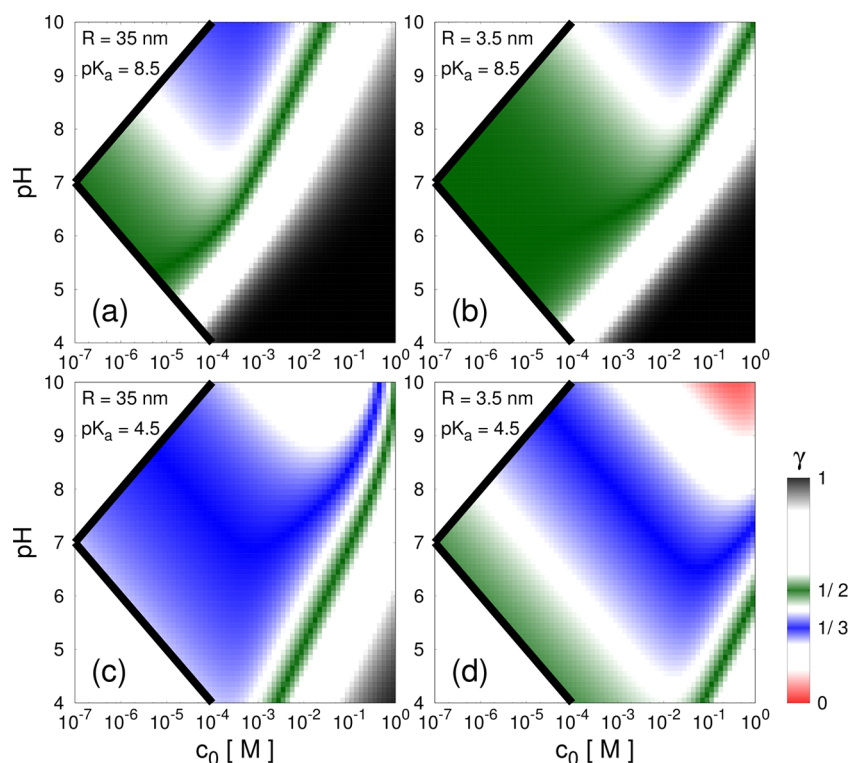


Figure 3. Color map of the local exponent γ [eq 27], calculated numerically by solving eq 1, in the c_0 -pH plane for nanotubes of $R = 35.0$ nm and $R = 3.5$ nm, using $pK_a = 4.5$ and 8.5 . Panels (a) and (d) correspond to the theoretical curves in Figure 2a and b, respectively. We use $\epsilon = 78$, $T = 298$ K, $\eta = 0.89$ mPa·s, $\nu_0 = 75$ cm²·S/(e·mol), and $\Gamma_{\text{site}} = 19/\text{nm}^2$.

we would need more experimental data. Also for $R = 3.5$ nm, shown in Figure 2b, the solid lines agree with the experimental data, except for $\text{pH} = 6$. Similar to the case of $R = 35$ nm, the solid lines of $\text{pH} = 10$ and 8 (red and blue) approach the broken lines ($\gamma = 1/3$), whereas the solid line and the experimental data of $\text{pH} = 4$ approach the dotted line ($\gamma = 1/2$), clearly showing the crossover of the exponent from $\gamma = 1/3$ to $1/2$.

To clarify how the appearance of the different power-law exponents in experimental data depends on pK_a and Γ_{site} , we show the color map of the exponent γ in the c_0 -pH plane in Figure 3 for the cases $R = 35$ and 3.5 nm and $pK_a = 8.5$ and 4.5 . For $R = 35$ nm and $pK_a = 8.5$, Figure 3a, corresponding to Figure 2a, a region with $\gamma = 0$ (red) does not appear and the region with $\gamma = 1/2$ (green) appears only at very low salinity, $c_0 < 10^{-4}$ M, and low pH. The green stripe between the regions with $\gamma = 1$ (black) and $\gamma = 1/3$ (blue) is transitional, so the conductivity plotted as a function of salinity does not clearly show the exponent $\gamma = 1/2$, in agreement with Figure 2a. For $R = 3.5$ nm and $pK_a = 8.5$, Figure 3b, the green region ($\gamma = 1/2$) becomes larger than the one in Figure 3a whereas the black and blue regions ($\gamma = 1, 1/3$) become smaller. This fact is understood by the shift of the boundaries [eqs 29 and 30] for small R . For $R = 35$ nm and $pK_a = 4.5$, Figure 3c, the green and black regions ($\gamma = 1/2, 1$) disappear whereas the blue region ($\gamma = 1/3$) becomes larger than the one in Figure 3a, which can be understood by the shift of the boundaries [eqs 29 and 31] for small pK_a . For $R = 3.5$ nm and $pK_a = 4.5$, Figure 3d, corresponding to Figure 2b, a region with $\gamma = 1$ (black) does not appear, meaning that the surface conductivity dominates the bulk conductivity even up to $c_0 = 1$ M. In contrast to Figure 3c, a red region ($\gamma = 1$) emerges because the boundary of eq 32 moves to the right.

CONCLUSIONS

On the basis of the Poisson–Boltzmann and hydrodynamic equations in cylindrical coordinates, we calculate the conductivity of single charged nanotubes filled with electrolyte. We use the co-ion-exclusion approximation and describe the crossover between the asymptotic behaviors theoretically. We analytically show the existence of four different power-law regimes with the exponents $\gamma = 0, 1/3, 1/2$, and 1 , in good agreement with the numerical solution of the full PB equation in cylindrical coordinates. Furthermore, we apply our theory to recent experimental results on carbon nanotube conductance. Using an estimated density of dissociable sites and fitted pK_a values for each radius, our theory agrees with the experimental data. For both radii, the experimental data exhibit the $\gamma = 1/3$ power law and at very low pH we find a crossover from $\gamma = 1/3$ to $1/2$. In general, our results show that the power-law exponent of the conductivity as a function of the reservoir salt concentration shows a succession of different values which depend sensitively on the nanotube radius R , the pH and the pK_a .

AUTHOR INFORMATION

Corresponding Author

*E-mail: d.j.bonthuis@fu-berlin.de (D.J.B.).

ORCID

Yuki Uematsu: 0000-0002-4970-4696

Notes

The authors declare no competing financial interest.

ACKNOWLEDGMENTS

The authors acknowledge funding from ANR, Projet de Recherche Collaborative – Internationale (PRCI) and the

Deutsche Forschungsgemeinschaft (DFG) via grant NE 810/11. Y.U. was supported by Grant-in-Aid for JSPS Fellows 16J00042.

REFERENCES

- (1) Stein, D.; Kruthof, M.; Dekker, C. Surface-Charge-Governed Ion Transport in Nanofluidic Channels. *Phys. Rev. Lett.* **2004**, *93*, 035901.
- (2) Dellago, C.; Naor, M. M.; Hummer, G. Proton Transport Through Water-Filled Carbon Nanotubes. *Phys. Rev. Lett.* **2003**, *90*, 105902.
- (3) Karnik, R.; Duan, C.; Castelino, K.; Daiguji, H.; Majumdar, A. Rectification of Ionic Current in a Nanofluidic Diode. *Nano Lett.* **2007**, *7*, 547–551.
- (4) Plecis, A.; Schoch, R. B.; Renaud, P. Ionic Transport Phenomena in Nanofluidics: Experimental and Theoretical Study of the Exclusion-Enrichment Effect on a Chip. *Nano Lett.* **2005**, *5*, 1147–1155.
- (5) Lee, C. Y.; Choi, W.; Han, J.-H.; Strano, M. S. Coherence Resonance in a Single-Walled Carbon Nanotube Ion Channel. *Science* **2010**, *329*, 1320–1324.
- (6) Choi, W.; Ulissi, Z. W.; Shimizu, S. F.; Bellisario, D. O.; Ellison, M. D.; Strano, M. S. Diameter-Dependent Ion Transport Through the Interior of Isolated Single-Walled Carbon Nanotubes. *Nat. Commun.* **2013**, *4*, 2397.
- (7) Ellison, M. D.; Menges, S.; Nebel, L.; D'Arcangelo, G.; Kramer, A.; Drahushuk, L.; Benck, J.; Shimizu, S.; Strano, M. S. Electrokinetic Transport of Methanol and Lithium Ions Through a 2.25-nm-Diameter Carbon Nanotube Nanopore. *J. Phys. Chem. C* **2017**, *121*, 2005–2013.
- (8) Van der Heyden, F. H. J.; Bonthuis, D. J.; Stein, D.; Meyer, C.; Dekker, C. Power Generation by Pressure-Driven Transport of Ions in Nanofluidic Channels. *Nano Lett.* **2007**, *7*, 1022.
- (9) Westermann-Clark, G. B.; Anderson, J. L. Experimental Verification of the Space-Charge Model for Electrokinetics in Charged Microporous Membranes. *J. Electrochem. Soc.* **1983**, *130*, 839–847.
- (10) Martinez, L.; Hernandez, A.; Ibáñez, J. A.; Tejerina, F. Study of Electrolyte Conductivity in Charged Microcapillary Porous Membranes. *Sep. Sci. Technol.* **1989**, *24*, 41–49.
- (11) Sakmann, B.; Trube, G. Conductance Properties of Single Inwardly Rectifying Potassium Channels in Ventricular Cells from Guinea-Pig Heart. *J. Physiol.* **1984**, *347*, 641–657.
- (12) Benz, R.; Schmid, A.; Wagner, W.; Goebel, W. Pore Formation by the Escherichia Coli Hemolysin: Evidence for an Association-Dissociation Equilibrium of the Pore-Forming Aggregates. *Infect. Immun.* **1989**, *57*, 887–895.
- (13) Trias, J.; Benz, R. Characterization of the Channel Formed by the Mycobacterial Porin in Lipid Bilayer Membranes. Demonstration of Voltage Gating and of Negative Point Charges at the Channel Mouth. *J. Biol. Chem.* **1993**, *268*, 6234–6240.
- (14) Smeets, R. M. M.; Keyser, U. F.; Krapf, D.; Wu, M.-Y.; Dekker, N. H.; Dekker, C. Salt Dependence of Ion Transport and DNA Translocation Through Solid-State Nanopores. *Nano Lett.* **2006**, *6*, 89–95.
- (15) Liu, H.; He, J.; Tang, J.; Liu, H.; Pang, P.; Cao, D.; Krstic, P.; Joseph, S.; Lindsay, S.; Nuckolls, C. Translocation of Single-Stranded DNA Through Single-Walled Carbon Nanotubes. *Science* **2010**, *327*, 64–67.
- (16) Pang, P.; He, J.; Park, J. H.; Krstić, P. S.; Lindsay, S. Origin of Giant Ionic Currents in Carbon Nanotube Channels. *ACS Nano* **2011**, *5*, 7277–7283.
- (17) Amiri, H.; Shepard, K. L.; Nuckolls, C.; Sánchez, R. H. Single-Walled Carbon Nanotubes: Mimics of Biological Ion Channels. *Nano Lett.* **2017**, *17*, 1204–1211.
- (18) Yazda, K.; Tahir, S.; Michel, T.; Loubet, B.; Manghi, M.; Bentin, J.; Picaud, F.; Palmeri, J.; Henn, F.; Jourdain, V. Voltage-Activated Transport of Ions Through Single-Walled Carbon Nanotubes. *Nano-scale* **2017**, *9*, 11976–11986.
- (19) Secchi, E.; Niguès, A.; Jubin, L.; Siria, A.; Bocquet, L. Scaling Behavior for Ionic Transport and Its Fluctuations in Individual Carbon Nanotubes. *Phys. Rev. Lett.* **2016**, *116*, 154501.
- (20) Biesheuvel, P. M.; Bazant, M. Z. Analysis of Ionic Conductance of Carbon Nanotubes. *Phys. Rev. E: Stat. Phys., Plasmas, Fluids, Relat. Interdiscip. Top.* **2016**, *94*, 050601.
- (21) Benham, C. J. The Cylindrical Poisson-Boltzmann Equation. I. Transformations and General Solutions. *J. Chem. Phys.* **1983**, *79*, 1969.
- (22) Donnan, F. G. Theorie Der Membrangleichgewichte Und Membranpotentiale Bei Vorhandensein Von Nicht Dialysierenden Elektrolyten. Ein Beitrag Zur Physikalisch-Chemischen Physiologie. *Z. Elektrochem. Angew. Phys. Chem.* **1911**, *17*, 572–581.
- (23) Levine, S.; Marriott, J. R.; Neale, G.; Epstein, N. Theory of Electrokinetic Flow in Fine Cylindrical Capillaries at High Zeta-Potentials. *J. Colloid Interface Sci.* **1975**, *52*, 136–149.
- (24) Balme, S.; Picaud, F.; Manghi, M.; Palmeri, J.; Bechelany, M.; Cabello-Aguilar, S.; Abou-Chaaya, A.; Miele, P.; Balanzat, E.; Janot, J. M. Ionic Transport Through Sub-10nm Diameter Hydrophobic High-Aspect Ratio Nanopores: Experiment, Theory and Simulation. *Sci. Rep.* **2015**, *5*, 10135.
- (25) Bonthuis, D. J.; Netz, R. R. Unraveling the Combined Effects of Dielectric and Viscosity Profiles on Surface Capacitance, Electro-Osmotic Mobility, and Electric Surface Conductivity. *Langmuir* **2012**, *28*, 16049–16059.
- (26) Bonthuis, D. J.; Netz, R. R. Beyond the Continuum: How Molecular Solvent Structure Affects Electrostatics and Hydrodynamics at Solid-Electrolyte Interfaces. *J. Phys. Chem. B* **2013**, *117*, 11397–11413.
- (27) Rice, C. L.; Whitehead, R. Electrokinetic Flow in a Narrow Cylindrical Capillary. *J. Phys. Chem.* **1965**, *69*, 4017–4024.
- (28) Manghi, M.; Palmeri, J.; Yazda, K.; Henn, F.; Jourdain, V. Role of Charge Regulation and Flow Slip on the Ionic Conductance of Nanopores: an Analytical Approach. **2017**, arXiv:1712.01055 condmat.soft.
- (29) Langmuir, I. The Adsorption of Gases on Plane Surface of Glass, Mica and Plantinum. *J. Am. Chem. Soc.* **1918**, *40*, 1361–1403.
- (30) Roger, K.; Cabane, B. Why Are Hydrophobic/Water Interfaces Negatively Charged? *Angew. Chem., Int. Ed.* **2012**, *51*, 5625–5628.
- (31) Grosjean, B.; Pean, C.; Siria, A.; Bocquet, L.; Vuilleumier, R.; Bocquet, M.-L. Chemisorption of Hydroxide on 2D Materials from DFT Calculations: Graphene Versus Hexagonal Boron Nitride. *J. Phys. Chem. Lett.* **2016**, *7*, 4695–4700.
- (32) Uematsu, Y.; Bonthuis, D. J.; Netz, R. R. Charged Surface-Active Impurities at Nanomolar Concentration Induce Jones-Ray Effect. *J. Phys. Chem. Lett.* **2018**, *9*, 189–193.
- (33) Healy, T. W.; Fuerstenau, D. W. The Isoelectric Point/Point-of-Zero-Charge of Interfaces Formed by Aqueous Solutions and Nonpolar Solids, Liquids, and Gases. *J. Colloid Interface Sci.* **2007**, *309*, 183–188.
- (34) Zuccaro, L.; Krieg, J.; Desideri, A.; Kern, K.; Balasubramanian, K. Tuning the Isoelectric Point of Graphene by Electrochemical Functionalization. *Sci. Rep.* **2015**, *5*, 11794.
- (35) Lau, A. C.; Furlong, D. N.; Healy, T. W.; Grieser, F. The Electrokinetic Properties of Carbon Black and Graphitized Carbon Black Aqueous Colloids. *Colloids Surf.* **1986**, *18*, 93–104.
- (36) Lee, C.; Joly, L.; Siria, A.; Biance, A.-L.; Fulcrand, R.; Bocquet, L. Large Apparent Electric Size of Solid-State Nanopores Due to Spatially Extended Surface Conduction. *Nano Lett.* **2012**, *12*, 4037–4044.
- (37) Hall, J. E. Access Resistance of a Small Circular Pore. *J. Gen. Physiol.* **1975**, *66*, 531–532.